Anal.Math.Phys. (2012) 2:347–366
DOI 10.1007/s13324-012-0040-7

A dispersive model for undular bores

Alfatih Ali · Henrik Kalisch

Received: 1 November 2011 / Accepted: 2 May 2012 / Published online: 12 October 2012

Abstract In this article, consideration is given to weak bores in free-surface flows. The energy loss in the shallow-water theory for an undular bore is thought to be due to upstream oscillations that carry away the energy lost at the front of the bore. Using a higher-order dispersive model equation, this expectation is confirmed through a quantitative study which shows that there is no energy loss if dispersion is accounted for.

Keywords Undular bore · Energy loss · Dispersion

1 Introduction

The bore is a well known phenomenon in fluid mechanics, describing the transition between two uniform streams with different flow depths. Depending on the strength of the bore, it may feature oscillations, breaking waves, or fully developed turbulence. The classical theory of bores due to Lord Rayleigh [38] uses mass and momentum conservation in the shallow-water equation to predict a loss of energy at the bore front. While it is generally accepted that the energy loss in a strong bore is due to turbulent dissipation, it appears that the precise nature of the energy loss in a weak bore has not been explained in a satisfactory manner. The accepted point of view is that the excess energy is disseminated by oscillations behind the bore front. However, as far as

This article is dedicated to the memory of our friend and colleague Vladimir Varlamov.

A. Ali · H. Kalisch (✉)
Department of Mathematics, University of Bergen, Postbox 7800, 5020 Bergen, Norway
e-mail: henrik.kalisch@math.uib.no

A. Ali
e-mail: alfatih.ali@math.uib.no

we know, this commonly held belief has as of yet not been confirmed by quantitative evidence. It is our purpose in this article to remedy this state of affairs by presenting a detailed study of undular bores using a dispersive theory.

More generally, we will derive expressions for mass, momentum and energy integrals in a nonlinear dispersive system of evolutions equations appearing in the context of the Boussinesq scaling. These integrals will be used in a numerical study of an undular bore, and it will become plain that conservation of mass, momentum and energy holds to the same order of accuracy as the equations are asymptotically valid.

While observations of bores abound, there are few field measurements available, so that one has to resort to laboratory experiments in order to obtain quantitative information. Here, we mention the early studies of Favre [27] and Binnie and Orkney [6], and the recent work of Chanson [17,18] and Koch and Chanson [33,34]. In [27], it was found that bores appear in different types. Undular bores feature free-surface oscillations behind the front of the bore, and we will say that a bore is purely undular, if none of the waves behind the bore are breaking. As found in [27], such purely undular bores occur if the ratio of the difference between upstream and downstream flow-depths against the undisturbed depth is less than about 0.28. Increasing the ratio beyond this value will result in one or a few waves breaking, and a value of 0.75 and beyond will result in a completely turbulent transition region.

Let us next give a short account of the works that have investigated the energy loss through undulations in a weak bore. One of the first to take up the problem was Lemoine [35]. Using a linear approach and assuming a sinusoidal wavetrain, Lemoine calculated the rate of radiation of energy from the bore front, but obtained only moderate agreement with experiments. Benjamin and Lighthill [5] argued that the ensuing wavetrain must be of cnoidal character. They showed that it is only possible to match a cnoidal periodic wavetrain to a uniform stream if there is a change in the volume flow rate, the momentum flow rate or the energy per unit mass, thus again leading to a loss of energy if both mass and momentum are to be conserved. Later, Sturtevant [39] used data from Favre's experiments [27] and a cnoidal wave approximation to argue that there must be a change in both momentum and energy due to the existence of a boundary layer below the bore. While dissipation undoubtedly plays a role, and may be as important as dispersion in an experimental setting, we argue that the energy loss predicted by the shallow-water system is not due to physical dissipation, but rather should be viewed as a failure of the shallow-water approximation to capture the precise transition between the two uniform streams. As it will turn out, a dispersive correction of the shallow-water system is sufficient to essentially eliminate the energy loss due to the inaccuracy of the shallow-water system.

To understand the mass, momentum and energy conservation in an undular bore, we use the weakly nonlinear dispersive model system

$$\begin{aligned} \eta_t + h_0 w_x + (w\eta)_x + \tfrac{h_0^3}{6} w_{xxx} &= 0, \\ w_t + g\,\eta_x + w w_x + \tfrac{g h_0^2}{6} \eta_{xxx} &= 0, \end{aligned} \tag{1.1}$$

where η represents the deflection of the free surface from its rest position, h_0 is the undisturbed fluid depth, and w denotes the horizontal flow velocity at a height $\sqrt{2/3}\,h_0$

above the flat bottom. As usual, g denotes the gravitational acceleration. Using (1.1), it will be shown that if dispersion is included into the model equations, then the energy loss mentioned above can be accounted for. Indeed, monitoring the mechanical energy associated to (1.1) shows that the rate of change of the energy contained in a control volume containing both the bore front and the ensuing oscillations is exactly equal to the net influx of energy, including both the flow rate of energy on either side, and the net work done by pressure forces on the control volume. Consequently, there is no energy loss if dispersion is accounted for. In particular, this shows there is no need for a further dissipative correction of the shallow-water system if dispersion is properly treated.

To compare our findings to previous studies presented in [5,39], we note that these works while taking account of dispersion, deal exclusively with the time-independent problem. Moreover, the (steady) KdV equation used in these works is limited to unidirectional propagation, thusly only taking account of waves propagating in the same direction as the bore. In contrast, we use a time-dependent system of equations allowing for counterpropagating waves. The unsteady problem has been investigated in [37] using a dispersive system similar to (1.1), but no study of the development of the energy was provided. More recently, bores have been studied in the context of another system also derived in [8], but more amenable to numerical methods [7,31], and even with the help of fully nonlinear evolutions equations [26,43]. A few examples of dissipative models for undular bores were studied in [15]. Energy issues in connection with the generation of tsunamis have been studied with a model similar to (1.1) in [23]. The findings of the present article have been announced in [3].

The basis for our study is the following free-surface problem. Consider an incompressible and inviscid fluid contained in a long narrow channel, such that the depth of the undisturbed fluid is h_0. If it is assumed that the fluid flow is irrotational and does not vary significantly in the direction transverse to the length of the channel, and that the free surface can be described by a single-valued function $\eta(x,t)$, then the free-surface problem can be written in terms of the Laplace equation for the velocity potential ϕ as follows.

$$\begin{aligned}
&\phi_{xx} + \phi_{zz} = 0, \quad \text{in } -h_0 < z < \eta(x,t),\\
&\phi_z = 0, \quad \text{at } z = -h_0,\\
&\eta_t + \phi_x \eta_x - \phi_z = 0, \quad \text{at } z = \eta(x,t),\\
&\phi_t + \tfrac{1}{2}(\phi_x^2 + \phi_z^2) + g\eta = 0, \quad \text{at } z = \eta(x,t).
\end{aligned}$$

Both the shallow-water and the dispersive system can be derived as limiting cases of this free-surface problem. In Sect. 2, we briefly describe the shallow-water theory, and its implications for the study of bores. The shallow-water approximation is used in river hydraulics and open channel flows, and despite its limitations, yields fairly accurate predictions [16,27,44].

A dispersive system of partial differential equations along with the corresponding momentum and energy integrals is derived in Sect. 3. Here it is imperative that the correct momentum and energy integrals be found. Careful considerations show that in the case of bore-type boundary conditions, the momentum and energy integrals

associated to (1.1) are in fact the same as the corresponding integrals associated to the shallow-water approximation.

Then, using the system (1.1) and the corresponding expressions for the mass, momentum and energy, numerical experiments are set up in Sect. 4 to understand the conservation properties of this approximation.

It is found that the flow quantities predicted by the dispersive system are similar to those predicted by the shallow-water theory. However, as mentioned above, the dispersive theory does not lead to the energy loss which is characteristic of the shallow-water theory. In the appendix, some details are given concerning the numerical procedure used to approximate solutions of the dispersive system (1.1).

2 Shallow water theory

In this section, we will recall the implications of the standard shallow-water theory when applied to a free-surface bore. If the transition between the upstream and downstream flow depths is gentle, and the undisturbed fluid depth is not too great, a long-wave approximation is justified. Equivalently, it may be assumed that the pressure is hydrostatic, and the horizontal velocity u does not depend on the vertical coordinate z. If this is done, the shallow-water system

$$\begin{aligned} \eta_t + h_0 u_x + (u\eta)_x &= 0, \\ u_t + g\eta_x + uu_x &= 0, \end{aligned} \tag{2.1}$$

appears as the governing set of equations for the fluid flow. As before, $\eta(x,t)$ is the deflection of the free surface from its rest position, and h_0 is the undisturbed fluid depth. However $u(x,t)$ now represents a uniform horizontal velocity. The system (2.1) has a well known weak solution accommodating the transition between the upstream and downstream uniform flows through a sudden jump. The surface profile η of this discontinuous solution is depicted in Fig. 1. Figure 1 also elucidates the geometric setup of the problem. Fluid of undisturbed depth h_0 running in a horizontal channel of uniform width over a flat bottom. Assuming that the shock is initially located at $x = 0$, the precise formula for the weak solution shown in Fig. 1 is

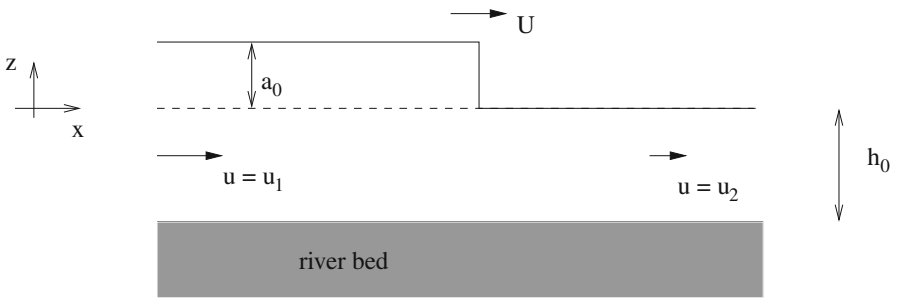

Fig. 1 Schematic of a discontinuous solution of (2.1). The velocity jumps from u_1 to u_2, and the amplitude jumps from $h_0 + a_0$ to h_0. The front of the bore moves upstream at a velocity U

$$\eta(x,t) = \begin{cases} a_0, & x < Ut, \\ 0, & x > Ut, \end{cases}$$
$$u(x,t) = \begin{cases} u_1, & x < Ut, \\ u_2, & x > Ut. \end{cases}$$

Here and in the following, it will be assumed that the upstream flow depth is the same as the undisturbed depth of the fluid. This is in accordance with experiments, where a discharge is imposed on a fluid at rest, or on a previously established uniform stream. Note also that the arrows in Fig. 1 point in the upstream direction, because river bores generally move upstream. Recall that smooth solutions of the system (2.1) conserve the mass, the momentum, and the energy of an initial state. Let h be the total depth of the fluid, given by $h(x,t) = h_0 + \eta(x,t)$. The conservation of mass in a control volume of unit width above the interval $[x_1, x_2]$ is expressed as

$$\frac{d}{dt}\int_{x_1}^{x_2} \rho h(x,t)\,dx = \rho u(x_1,t)h(x_1,t) - \rho u(x_2,t)h(x_2,t). \tag{2.2}$$

Similarly, the conservation of momentum is given by

$$\frac{d}{dt}\int_{x_1}^{x_2} \rho u(x,t)h(x,t)\,dx = \rho u^2(x_1,t)h(x_1,t) - \rho u^2(x_2,t)h(x_2,t) + \frac{\rho}{2}gh^2(x_1,t) - \frac{\rho}{2}gh^2(x_2,t). \tag{2.3}$$

The energy associated to the shallow-water approximation is given by the integral

$$E(\eta,u) = \frac{\rho}{2}\int_{x_1}^{x_2} \left\{u^2(x,t)h(x,t) + gh^2(x,t)\right\} dx, \tag{2.4}$$

while the energy influx at x_i is given by

$$F_i = \frac{\rho}{2}u^3(x_i,t)h(x_i,t) + \rho g u(x_i,t)h^2(x_i,t), \tag{2.5}$$

where ρ is the density of the fluid. Note that the second term in F_i comprises both the energy flow rate and the work done by the pressure force, and therefore the quantity $F_1 - F_2$ represents the net influx of energy into a control volume of unit width, delimited by the interval $[x_1, x_2]$.

Now the solution indicated in Fig. 1 is not continuous, so that the integrals for mass, momentum and energy are not differentiable. However, one may still impose conservation of mass and momentum, which when applied to the exact form of the

weak solution yields the following shock conditions [44].

$$\begin{aligned} U\Big[h(x_2,t)-h(x_1,t)\Big] &= \Big[h(x_2,t)u(x_2,t)-h(x_1,t)u(x_1,t)\Big],\\ U\Big[h(x_2,t)u(x_2,t)-h(x_1,t)u(x_1,t)\Big] &= \Big[h(x_2,t)u^2(x_2,t)-h(x_1,t)u^2(x_1,t)\Big]\\ &\quad +\frac{g}{2}\Big[h^2(x_2,t)-h^2(x_1,t)\Big]. \end{aligned}$$

Given the upstream velocity $u_2 = u(x_2,t)$, and the downstream flow depth $h(x_1,t) = h_0 + a_0$, these equations define the velocity U of the front of the bore by

$$U = u_2 + \sqrt{\frac{g}{2h_0}\big(2h_0^2 + 3a_0h_0 + a_0^2\big)}, \tag{2.6}$$

and the initial flow velocity at $x = x_1$ as

$$u_1 = u_2 + \frac{a_0}{a_0+h_0}\sqrt{\frac{g}{2h_0}\big(2h_0^2 + 3a_0h_0 + a_0^2\big)}. \tag{2.7}$$

The loss of energy across the bore may be computed exactly. Denoting the upstream and downstream energy fluxes by F_2 and F_1, respectively, and denoting the total mechanical energy contained in the fluid region between x_1 and x_2, we find the equation

$$-\frac{dE(\eta,u)}{dt} + (F_1 - F_2) = \frac{a_0^3}{4}\,\rho\sqrt{\tfrac{1}{2}\,g^3\,\Big(\tfrac{1}{h_0}+\tfrac{1}{a_0+h_0}\Big)}. \tag{2.8}$$

The right-hand side of this equation represents the energy lost due the approximate nature of the governing Eq. (2.1) and the discontinuous solutions.

3 The dispersive model

In this section, a dispersive model equation is derived from the full water-wave problem for surface waves over a flat bottom. Assuming irrotational flow of an incompressible inviscid fluid, the surface water-wave problem is given in terms of the velocity potential $\phi(x,z,t)$ and the surface profile $\eta(x,t)$ as stated in the introduction. As explained in [44], assuming the expansion

$$\phi = \sum_{n=0}^{\infty} z^n f_n(x,t),$$

the Laplace equation for ϕ and the bottom boundary condition yield

$$\phi = \sum_{m=0}^{\infty}(-1)^m \frac{z^{2m}}{(2m)!}\frac{\partial^{2m} f}{\partial x^{2m}},$$

where $f = f_0$. In the following it will be necessary to use a typical amplitude and wavelength of the waves to be described. While a_0 is an obvious choice for a typical amplitude, we choose a space scale ℓ, which is not a priori given by the problem. Non-dimensional variables are defined by

$$\tilde{x} = \frac{1}{\ell}\, x, \quad \tilde{z} = \frac{1}{h_0}(z + h_0), \quad \tilde{\eta} = \frac{1}{a_0}\, \eta, \quad \tilde{t} = \frac{c_0}{\ell}\, t, \quad \tilde{\phi} = \frac{c_0}{g\ell a_0}\, \phi,$$

where $c_0 = \sqrt{gh_0}$ is the limiting long-wave speed. In terms of the two small parameters $\alpha = \frac{a_0}{h_0}$ and $\beta = \frac{h_0^2}{\ell^2}$, which are assumed to be of the same order of magnitude, the non-dimensional problem is

$$\begin{aligned}
\beta\, \tilde{\phi}_{\tilde{x}\tilde{x}} + \tilde{\phi}_{\tilde{z}\tilde{z}} &= 0, \quad \text{in } 0 < \tilde{z} < 1 + \alpha\tilde{\eta}, \\
\tilde{\phi}_{\tilde{z}} &= 0, \quad \text{at } \tilde{z} = 0, \\
\tilde{\eta}_{\tilde{t}} + \alpha\tilde{\phi}_{\tilde{x}}\tilde{\eta}_{\tilde{x}} - \tfrac{1}{\beta}\tilde{\phi}_{\tilde{z}} &= 0, \quad \text{at } \tilde{z} = 1 + \alpha\tilde{\eta}, \\
\tilde{\phi}_{\tilde{t}} + \tfrac{1}{2}\alpha\tilde{\phi}_{\tilde{x}}^2 + \tfrac{\alpha}{\beta}\tilde{\phi}_{\tilde{z}}^2 + \tilde{\eta} &= 0, \quad \text{at } \tilde{z} = 1 + \alpha\tilde{\eta}.
\end{aligned}$$

Scaling the previous expansion for ϕ, we find that

$$\begin{aligned}
\tilde{\phi} &= \sum_{m=0}^{\infty} (-1)^m \frac{\tilde{z}^{2m}}{(2m)!} \frac{\partial^{2m} \tilde{f}}{\partial \tilde{x}^{2m}} \beta^m \\
&= \tilde{f} - \beta \frac{\tilde{z}^2}{2} \tilde{f}_{\tilde{x}\tilde{x}} + \beta^2 \frac{\tilde{z}^4}{4!} \tilde{f}_{\tilde{x}\tilde{x}\tilde{x}\tilde{x}} + O(\beta^3),
\end{aligned}$$

where f is non-dimensionalized with the same factor as ϕ. Substituting the previous expression into the nondimensional surface boundary conditions yields

$$\begin{aligned}
\tilde{\eta}_t + \tilde{v}_{\tilde{x}} + \alpha(\tilde{\eta}\tilde{v})_{\tilde{x}} - \tfrac{1}{6}\beta\tilde{v}_{\tilde{x}\tilde{x}\tilde{x}} &= O(\alpha^2, \alpha\beta, \beta^2), \\
\tilde{\eta}_{\tilde{x}} + \tilde{v}_{\tilde{t}} - \tfrac{1}{2}\beta\tilde{v}_{\tilde{x}\tilde{x}\tilde{t}} + \alpha\tilde{v}\tilde{v}_{\tilde{x}} &= O(\alpha^2, \alpha\beta, \beta^2),
\end{aligned} \tag{3.1}$$

where $\tilde{v} = \tilde{f}_{\tilde{x}}$ connotes the non-dimensional horizontal velocity at the bottom. The velocity $\tilde{w}$ at the non-dimensional height $\sqrt{\frac{2}{3}}$ above the flat bottom is related to $\tilde{v}$ by

$$\tilde{v} = \tilde{w} + \tfrac{1}{3}\beta\tilde{w}_{\tilde{x}\tilde{x}} + O(\beta^2). \tag{3.2}$$

Substituting this relation into Eq. (3.1) yields

$$\begin{aligned}
\tilde{\eta}_{\tilde{t}} + \tilde{w}_{\tilde{x}} + \alpha(\tilde{\eta}\tilde{w})_{\tilde{x}} + \tfrac{1}{2}(\tfrac{2}{3} - \tfrac{1}{3})\beta\tilde{w}_{\tilde{x}\tilde{x}\tilde{x}} &= O(\alpha^2, \alpha\beta, \beta^2), \\
\tilde{w}_{\tilde{t}} + \tilde{\eta}_{\tilde{x}} + \alpha\tilde{w}\tilde{w}_{\tilde{x}} + \tfrac{1}{2}\beta\left(\tfrac{2}{3} - 1\right)\tilde{w}_{\tilde{x}\tilde{x}\tilde{t}} &= O(\alpha^2, \alpha\beta, \beta^2).
\end{aligned}$$

Differentiating the lowest order approximation $\tilde{\eta}_{\tilde{x}} + \tilde{w}_{\tilde{t}} = O(\alpha, \beta)$, using this relation in the last term of the second equation, and disregarding terms of order α^2, $\alpha\beta$, and β^2, yields the final system

$$\tilde{\eta}_{\tilde{t}} + \tilde{w}_{\tilde{x}} + \alpha(\tilde{\eta}\tilde{w})_{\tilde{x}} + \tfrac{1}{6}\beta\tilde{w}_{\tilde{x}\tilde{x}\tilde{x}} = 0,$$
$$\tilde{w}_{\tilde{t}} + \tilde{\eta}_{\tilde{x}} + \alpha\tilde{w}\tilde{w}_{\tilde{x}} + \tfrac{1}{6}\beta\tilde{\eta}_{\tilde{x}\tilde{x}\tilde{x}} = 0.$$

In dimensional variables, the system (1.1) appears. Note that for very long waves, the coefficient β is nearly zero, so that the system (1.1) reduces to the shallow-water system. More details of this derivation are given in [44]. We mention in passing that the transformations mentioned above may be used in a more systematic way to derive a general dispersive system [8]. Indeed, there are many different types of systems and equations of Boussinesq type, such as the single Boussinesq fourth-order equation [2,32], higher-order and two-dimensional systems [36,40,42], damped systems [41], and systems arising in elasticity [22]. There are also many papers featuring comparison of solutions of different nonlinear dispersive evolutions equations and with experiments in wave tanks [1,12,13]. However, our present focus is on the system (1.1), and we now continue to find the important mass, momentum and energy integrals associated with the system (1.1).

The mass per unit width of the fluid contained in the control volume delimited by the interval $[x_1, x_2]$ is given by

$$m = \rho \int_{x_1}^{x_2} \int_{-h_0}^{\eta} dz\, dx = \rho \int_{x_1}^{x_2} (\eta + h_0)\, dx. \tag{3.3}$$

The horizontal momentum per unit width of the fluid contained in the same control volume is given by

$$M = \rho \int_{x_1}^{x_2} \int_{-h_0}^{\eta} \phi_x(x, z)\, dz\, dx.$$

Rescaling and using the approximation for $\tilde{\phi}$, the momentum is expressed as

$$M = \rho \frac{g\ell a}{c_0} h_0 \int_{x_1/\ell}^{x_2/\ell} \int_{0}^{1+\alpha\tilde{\eta}} \left\{ \tilde{f}_{\tilde{x}} - \beta \frac{\tilde{z}^2}{2} \tilde{f}_{\tilde{x}\tilde{x}\tilde{x}} + O(\beta^2) \right\} d\tilde{z}\, d\tilde{x}$$
$$= \rho\ell a c_0 \int_{x_1/\ell}^{x_2/\ell} \left\{ \tilde{f}_{\tilde{x}} + \alpha \tilde{f}_{\tilde{x}}\tilde{\eta} - \frac{\beta}{6} \tilde{f}_{\tilde{x}\tilde{x}\tilde{x}} + O(\beta^2, \alpha^2, \alpha\beta) \right\} d\tilde{x}.$$

The dimensionless momentum is approximated by

$$\tilde{M} = \frac{M}{\rho\ell a c_0} = \int_{x_1/\ell}^{x_2/\ell} \left\{ \tilde{f}_{\tilde{x}} + \alpha \tilde{f}_{\tilde{x}}\tilde{\eta} - \frac{\beta}{6} \tilde{f}_{\tilde{x}\tilde{x}\tilde{x}} \right\} d\tilde{x}.$$

In terms of $\tilde{w}$, this becomes

$$\tilde{M} = \int_{x_1/\ell}^{x_2/\ell} \left\{ \tilde{w} + \alpha \tilde{w}\tilde{\eta} + \frac{\beta}{6}\tilde{w}_{\tilde{x}\tilde{x}} \right\} d\tilde{x}.$$

Notice that for very long waves β is nearly zero, and the momentum reduces to the corresponding expression for the shallow-water approximation given in dimensional variables in (2.3).

To find the mechanical energy integral corresponding to the approximation which yields Eq. (1.1), we investigate the expression

$$E = E_K + E_P = \frac{1}{2}\rho \int_{x_1}^{x_2} \int_{-h_0}^{\eta} |\nabla\phi|^2 dz\, dx + \rho g \int_{x_1}^{x_2} \int_{-h_0}^{\eta} (z + h_0)\, dz\, dx,$$

where E_K denotes the kinetic energy, and E_P denotes the potential energy. To obtain an approximation for the total energy that corresponds to the model (1.1), we use the same scaling as before. The potential energy is given by

$$\begin{aligned} E_P &= \rho g h_0^2 \ell \int_{x_1/\ell}^{x_2/\ell} \int_0^{1+\alpha\tilde{\eta}} \tilde{z}\, d\tilde{z}\, d\tilde{x} \\ &= \frac{\rho g h_0^2 \ell}{2} \int_{x_1/\ell}^{x_2/\ell} \left\{ 1 + 2\alpha\tilde{\eta} + \alpha^2\tilde{\eta}^2 \right\} d\tilde{x}. \end{aligned}$$

The kinetic energy is

$$\begin{aligned} E_K &= \frac{\rho}{2}\left(\frac{g\ell a}{c_0}\right)^2 h_0 \ell \int_{x_1/\ell}^{x_2/\ell} \int_0^{1+\alpha\tilde{\eta}} \left\{ \tfrac{1}{\ell^2}\tilde{\phi}_{\tilde{x}}^2 + \tfrac{1}{h_0^2}\tilde{\phi}_{\tilde{z}}^2) \right\} d\tilde{z}\, d\tilde{x} \\ &= \alpha^2 \frac{\rho g h_0^2 \ell}{2} \int_{x_1/\ell}^{x_2/\ell} \int_0^{1+\alpha\tilde{\eta}} \left\{ \tilde{\phi}_{\tilde{x}}^2 + \tfrac{1}{\beta}\tilde{\phi}_{\tilde{z}}^2 \right\} d\tilde{z}\, d\tilde{x}. \end{aligned}$$

By substituting the expression for $\tilde{\phi}$ into the last integral, we see that the kinetic energy is

$$E_K = \alpha^2 \frac{\rho g h_0^2 \ell}{2} \int_{x_1/\ell}^{x_2/\ell} \left\{ \tilde{f}_{\tilde{x}}^2 + \alpha\tilde{\eta}\tilde{f}_{\tilde{x}}^2 - \tfrac{\beta}{3}\tilde{f}_{\tilde{x}}\tilde{f}_{\tilde{x}\tilde{x}\tilde{x}} + \tfrac{\beta}{3}\tilde{f}_{\tilde{x}\tilde{x}}^2 + O(\alpha^2, \alpha\beta, \beta^2) \right\} d\tilde{x}.$$

Now recognizing $\tilde{f}_{\tilde{x}}$ as $\tilde{v}$, using (3.2), and disregarding terms of order $\alpha^3\beta$ and $\alpha^2\beta^2$ it appears that

$$E_K = \alpha^2 \frac{\rho g h_0^2 \ell}{2} \int_{x_1/\ell}^{x_2/\ell} \left\{ \tilde{w}^2 + \alpha \tilde{\eta} \tilde{w}^2 + \tfrac{\beta}{3} \tilde{w} \tilde{w}_{\tilde{x}\tilde{x}} + \tfrac{\beta}{3} \tilde{w}_{\tilde{x}}^2 \right\} d\tilde{x}.$$

We now use the factor $\rho g h_0^2 \ell$ to nondimensionalize the energy. Then the total energy is given in non-dimensional form by the expression

$$\begin{aligned} \tilde{E} = \frac{E}{\rho g h_0^2 \ell} = \frac{\alpha^2}{2} \int_{x_1/\ell}^{x_2/\ell} \left\{ \tilde{w}^2 + \alpha \tilde{\eta} \tilde{w}^2 + \tfrac{\beta}{3} \tilde{w} \tilde{w}_{xx} + \tfrac{\beta}{3} \tilde{w}_x^2 \right\} d\tilde{x} \\ + \frac{1}{2} \int_{x_1/\ell}^{x_2/\ell} \left\{ 1 + 2\alpha \tilde{\eta} + \alpha^2 \tilde{\eta}^2 \right\} d\tilde{x}. \end{aligned}$$

Examining the expression (2.4) for the energy in the shallow-water theory, it appears that it contains terms of third-order. The inclusion of these terms can be explained by our desire to compare the result with the conserved quantities associated to the shallow-water system. Indeed, we see that in order to obtain the correct energy for the shallow-water system in the limit of small β, we have to include terms of order up to α^3 in the energy formula. These higher-order corrections do not change the order of accuracy of the energy integral, which is correct to second-order in α and β, but they facilitate the comparison with the shallow-water theory. A somewhat different approach to finding quantities such as M and E has been presented in [4].

In the preceding analysis, it was important to have knowledge of the approximate fluid velocity below a given surface wave. Such an approach may also be used to study the motion of individual particles in fluid flow associated to surface waves described by equations of Boussinesq type [14]. Certain properties of the fluid flow below a surface wave can also be understood in the context of the free-surface problem for the full Euler equations which was recalled in the introduction. Some recent results on fluid flow below steady surface waves can be found in [20,21,24,25,29,30].

4 Numerical study

The considerations presented in the previous section are now applied to the study of an undular bore. After a brief glance at the qualitative properties of the approximation provided here, i.e. the shape of the free surface, we will use the expressions for mass, momentum and energy found in the previous section to gain an understanding of the conservation properties of the undular bore, and in particular of the differences between the shallow-water system (2.1) and the model system (1.1). First, let us fix ideas regarding the expressions of mass, momentum and energy in the approximation which yields the model system (1.1). While the formula for mass conservation is already given in dimensional form, we note that the dimensional expressions for momentum and energy found in the last section are

$$M = \rho \int_{x_1}^{x_2} \left\{ (h_0 + \eta)w + \tfrac{h_0^3}{6} w_{xx} \right\} dx, \tag{4.1}$$

and

$$E = \frac{\rho}{2} \int_{x_1}^{x_2} \left\{ (h_0 + \eta)w^2 + g(h_0^2 + 2h_0\eta + \eta^2) + \tfrac{h_0^3}{3} w w_{xx} + \tfrac{h_0^3}{3} w_x^2 \right\} dx, \tag{4.2}$$

respectively. Recall that these integrals represent the momentum and energy contained in a section of unit width of the fluid above the interval $[x_1, x_2]$. If the interval $[x_1, x_2]$ is large enough to contain the bore front as well as any disturbances propagating away from the front, it is reasonable to assume that the values of the functions w and η at the endpoints x_1 and x_2 have settled to the far-field conditions of the respective uniform streams. In particular, this assumption encompasses zero spatial derivatives for both η and w. Now it appears that an integration by parts will help reduce the formula for E to the corresponding shallow-water energy as given in (2.4). Similar considerations show that the momentum integral M will also reduce to the shallow-water momentum, as written in (2.3). We are thus in the situation where instead of η and u, we use η and w as the primary dependent variables of the flow. However, the correct expressions for the mass, momentum and energy are the same as in the shallow-water theory. To distinguish between the different variables, we adopt the notation $E(\eta, u)$ for the energy associated to the shallow-water system, and $E(\eta, w)$ for the energy associated to the dispersive system (1.1). A similar convention will be in force for the mass integral m and the momentum integral M. Next note that in the case where the far-field conditions are the same as the boundary conditions and include zero spatial derivatives for both η and w, the mass flux associated with the system (1.1) reduces to the expression of the shallow-water theory given in (2.2). Thus the first equation in (1.1) may be used to find that

$$\begin{aligned} \frac{dm(\eta, w)}{dt} &= -\rho \int_{x_1}^{x_2} \{h_0 w_x + (w\eta)_x\}\, dx \\ &= \rho w(x_1, t)(h_0 + \eta(x_1, t)) - \rho w(x_2, t)(h_0 + \eta(x_2, t)), \end{aligned}$$

so that mass is exactly conserved in the approximation of (1.1) if the boundary conditions are appropriate. Similarly, momentum conservation follows from using both equations in (1.1) and zero Neumann conditions.

$$\begin{aligned} \frac{dM(\eta, w)}{dt} &= -\rho \int_{x_1}^{x_2} \{2h_0 w w_x + g h_0 \eta_x + g\eta\eta_x + (w\eta)_x + w\eta w_x\}\, dx \\ &= \rho h_0 \left[w^2(x_1, t) - w^2(x_2, t) \right] + \frac{\rho}{2} g \left[(\eta(x_1, t) + h_0)^2 - (\eta(x_2, t) + h_0)^2 \right] \\ &\quad + \rho\eta(x_1, t) w^2(x_1, t) - \rho\eta(x_2, t) w^2(x_2, t), \end{aligned}$$

and the right-hand side is recognized as the net momentum flux in the shallow-water theory. In order to find the influx and outflux of energy into and out of the control volume, we also use the previous assumption that the interval $[x_1, x_2]$ is sufficiently large, and that the flux is given by the expression (2.5) associated to the shallow-water system. As it appears that energy conservation is not exact in the framework of (1.1), we now embark upon a quantitative study of energy conservation in an undular bore in the framework of the system (1.1).

There are a number of ways to induce a bore in an experimental setting. One may impose a discharge onto a fluid at rest, or on a previously established uniform background flow which may be directed either in the direction of propagation of the bore front, or in the opposite direction [6,27,33]. As mentioned before, and indicated in Fig. 1, we may choose a reference frame in which the transition is from the undisturbed fluid level h_0 upstream of the bore to a prescribed fluid level h_0+a_0 downstream of the bore. If also the upstream flow u_2 is given then the shallow-water theory may be used to obtain approximate values for the downstream velocity u_1 and the bore velocity U.

Since most configurations can be described in terms of the nondimensional number $\alpha = \frac{a_0}{h_0}$ which indicates the strength of the bore, we perform all experiments with a depth $h_0 = 1$ m, and vary only the amplitude a_0. The initial position of the bore front is considered to be at the origin, and we take $x_1 << 0$, and $x_2 >> 0$, so that the boundary conditions can be chosen to be the same as the far field conditions, viz

$$\begin{aligned} \eta(x_1,t) &= a_0, \qquad \eta(x_2,t) = 0,\\ w(x_1,t) &= u_1, \qquad w(x_2,t) = u_2, \end{aligned}$$

where u_1 is related to a_0 and the undisturbed depth h_0 by formula (2.7). In addition, two Neumann conditions are required since the equations contain terms with third-order spatial derivatives. Since $x_1 << 0$ and $x_2 >> 0$, it can be assumed that all first spatial derivatives are in fact zero at the boundaries. The initial shape of the free surface $\eta_0(x)$ and the initial velocity $w_0(x)$ are given by

$$\begin{aligned} \eta_0(x) &= \tfrac{1}{2}a_0\big(1-\tanh(kx)\big),\\ w_0(x) &= u_2 + \tfrac{1}{2}(u_1-u_2)\big(1-\tanh(kx)\big). \end{aligned}$$

The modeling parameter k denotes the steepness of the initial bore slope. For a large enough interval, the initial conditions match the boundary conditions to machine precision. The numerical treatment is based on a finite-difference approximation, and will be detailed in the appendix. As will be shown in the appendix, the algorithm converges with the expected 2-nd order convergence rate.

A typical wave profile and the corresponding velocity distribution are shown in Fig. 2. As expected, the dispersive terms contribute to creating a wavetrain following the bore front. Here it is interesting to note that if the linear wave equation were to be used, one would need the relation $w \sim \frac{c_0}{g}\eta$, while in the one-directional (KdV) theory, the relation $w = \frac{g}{c_0}\eta - \frac{1}{4}\frac{g}{c_0 h_0}\eta^2$ is required. Indeed, both relations are approximately satisfied for very small values of the ratio $\frac{a_0}{h_0}$. However, as Fig. 3 shows, the deviation

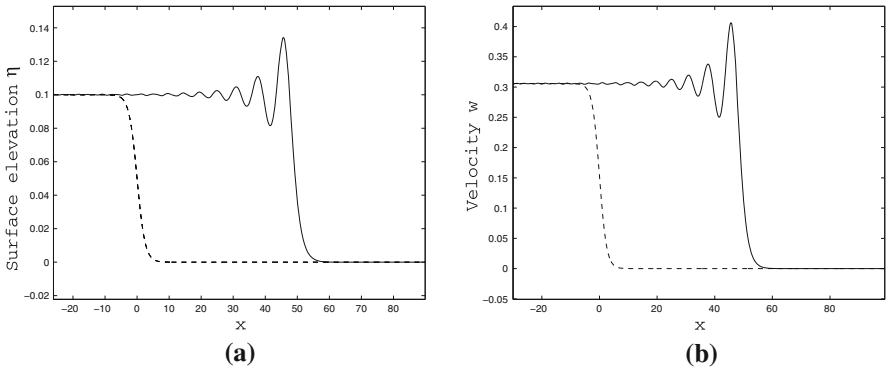

Fig. 2 Snapshot of the development of an undular bore at time $t = 15$s, with initial amplitude $a_0 = 0.1$m, and undisturbed depth $h_0 = 1$ m. **a** free surface η, **b** flow velocity w

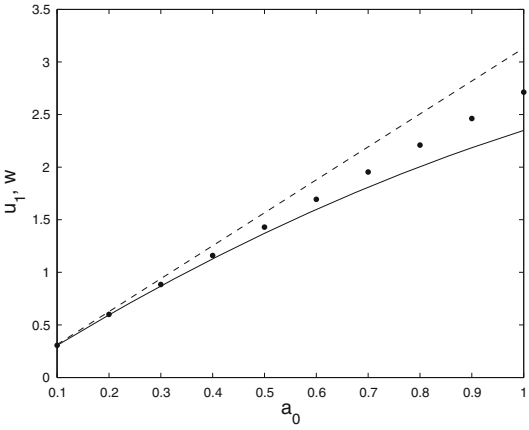

Fig. 3 Comparison of the left boundary condition for undisturbed depth $h_0 = 1$ m and upstream flow velocity $u_2 = 0$. The *dots* represent u_1, given by the shallow-water theory as in (2.7). The *dashed line* represents the first-order relation $w = \frac{g}{c_0}\eta$, while the *solid line* represents the second-order relation $w = \frac{g}{c_0}\eta - \frac{1}{4}\frac{g}{c_0 h_0}\eta^2$

between the present theory and the KdV theory grows significantly with increasing amplitude.

Let us now turn to the study of conservation properties of the dispersive system (1.1). As shown in Fig. 4, the energy loss experienced by the dispersive system is much smaller than the energy loss in the shallow-water system, albeit somewhat dependent on the model parameter k. Moreover, apart from a slight build-up of inaccuracy over time, we observe that the energy loss is nearly constant over time, so that we may summarize the energy loss for different bore strengths using a table. Table 1 shows the calculation of the energy rates for undular bores with different initial amplitudes a_0. As the amplitude of the undular bore increases, the percentage of the energy loss in the shallow-water approximation increases. In principle, the shallow-water approximation is not restricted to small-amplitude waves. However, even though the dispersive theory *is* restricted to small-amplitude waves, it gives much better results, even when applied outside of its range of applicability. Indeed, monitoring the energy as given by the integral (4.2) shows that the rate of change of $E(\eta, w)$ is exactly equal to the

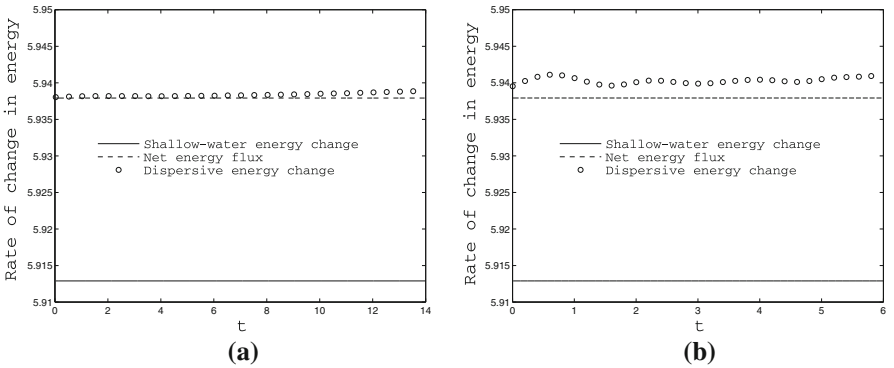

Fig. 4 Comparison of the rate of change of energy in the dispersive and the shallow-water system, versus the net energy change at the boundaries. The initial bore amplitude is $a_0 = 0.15\,\mathrm{m}$ and the undisturbed depth is $h_0 = 1\,\mathrm{m}$. **a** $k = 0.2$, **b** $k = 0.7$

Table 1 Column 1 shows the non-dimensional bore amplitude $\alpha = a_0/h_0$

α	$F_1 - F_2(\mathrm{kg\,m^2/s^3})$	$\frac{d}{dt}E(\eta, w)(\mathrm{kg\,m^2/s^3})$	$\frac{d}{dt}E(\eta, u)(\mathrm{kg\,m^2/s^3})$	Difference (%)
0.1	3.64	3.64	3.63	0.2
0.2	8.58	8.58	8.53	0.7
0.3	15.07	15.08	14.88	1.3
0.4	23.35	23.36	22.90	1.9
0.5	33.69	33.69	32.81	2.6
0.6	46.35	46.35	44.86	3.2
0.7	61.63	61.63	59.29	3.8

The net energy flux is shown in Column 2. Columns 3 and 4 display the rate of change in the energy of the dispersive theory and the shallow-water theory, respectively. Column 5 shows the percentage difference between the net energy flux and the rate of change of the shallow-water energy. The dispersive theory gives the correct result to within less than 0.1 % error

net influx of energy into the interval. It appears that the energy loss incurred by the shallow-water approximation is successfully captured by the dispersive system, and no dissipation mechanism is necessary to account for energy loss predicted by the shallow-water theory. Our findings effectively confirm the expectation that the excess energy is radiated by the continuous creation of waves.

Similar results obtain in cases where the bore is superimposed onto a background flow. We just briefly present the results of a computation where $u_2 = -2\,\mathrm{m/s}$. As can be seen in Table 2, the energy loss predicted by the shallow-water system is by far greater in relative terms than in the previous case where the bore was propagating into a fluid at rest. Again, the energy loss in the dispersive system is negligible, showing that the dispersive approximation successfully captures the energy loss also when a background flow is present.

Finally, Table 3 presents a comparison of net momentum flux, and bore front velocity in the shallow-water and dispersive theories in the case of a bore propagating into an

Table 2 Comparison of the change in energy in the shallow-water and dispersive systems when a strong backflow $u_2 = -2$ m/s is present

α	$F_1 - F_2$(kg m^2/s^3)	$\frac{d}{dt}E(\eta, w)$(kg m^2/s^3)	$\frac{d}{dt}E(\eta, u)$(kg m^2/s^3)	Difference (%)
0.1	0.836	0.836	0.829	0.84
0.2	2.170	2.187	2.128	1.93
0.3	4.200	4.201	4.005	4.87
0.4	7.036	7.034	6.582	6.48
0.5	10.86	10.87	9.992	7.92
0.6	15.87	15.88	14.38	9.38
0.7	22.26	22.27	19.92	10.51

Column 1 shows the non-dimensional bore amplitude $\alpha = a_0/h_0$. The net energy flux is shown in Column 2. Columns 3 and 4 display the rate of change in the energy of the dispersive theory and the shallow-water theory, respectively. Column 5 shows the percentage difference between the net energy flux and the rate of change of the shallow-water energy. The dispersive theory gives the correct result to within less than 0.3 % error

Table 3 Comparison of momentum change and bore velocities in the case when $u_2 = 0$

α	Net momentum flux (kg m/s^2)	$\frac{d}{dt}M(\eta, w)$ (kg m/s^2)	$\frac{d}{dt}M(\eta, u)$ (kgm/s^2)	U_{disp} (m/s)	U (m/s)	u_1 (m/s)
0.1	1.13	1.13	1.13	3.31	3.36	0.31
0.2	2.59	2.59	2.59	3.54	3.60	0.60
0.3	4.40	4.40	4.40	3.73	3.82	0.88
0.4	6.59	6.59	6.59	3.95	4.07	1.16
0.5	9.19	9.19	9.19	4.19	4.29	1.43
0.6	12.23	12.23	12.23	4.37	4.52	1.69
0.7	15.74	15.74	15.74	4.60	4.74	1.95

The net momentum flux is shown in Column 2. The change in momentum in the dispersive system and in the shallow-water system are shown in Columns 3 and 4 respectively. Columns 5 and 6 show the respective velocities U_{disp} and U of the bore front in the dispersive and shallow-water theory. Column 7 shows the far-field velocity u_1 of the uniform stream on the left

undisturbed fluid. As can be seen, the values for the change in momentum agree with the net influx of momentum in both the shallow-water, and the dispersive theory. Since we know that momentum is conserved exactly by the Eq. (1.1) the agreement here is another check on the validity of the numerical discretization. The velocity U_{disp} is obtained by following the inflection point at the bore front, and computing its velocity numerically. Some variations are visible in the bore front velocity, indicating that the bore front has a slightly smaller velocity in the dispersive theory.

Acknowledgments This work was supported in part by the Research Council of Norway. The authors would like to thank Professor John Albert for helpful comments.

Appendix A: The numerical scheme

The numerical discretization used to find approximate solutions of the system (1.1) is briefly presented. First, it should be noted that mathematical aspects of the system (1.1) have been studied in [9,11,28]. In these works, a theory of well posedness for the Cauchy problem and various boundary-value problems has been developed. In [10], a finite-element method for the periodic problem was constructed. Here, we consider a finite-difference method. We begin by writing $\zeta(x,t) = \eta(x,t) - \eta_0(x)$, and $\xi(x,t) = w(x,t) - w_0(x)$, so that the functions ζ and ξ satisfy homogeneous Dirichlet boundary conditions. Next, we use the transformation

$$\begin{pmatrix} u \\ v \end{pmatrix} = \begin{pmatrix} \sqrt[4]{\frac{g}{h_0}} & \sqrt[4]{\frac{h_0}{g}} \\ \sqrt[4]{\frac{g}{h_0}} & -\sqrt[4]{\frac{h_0}{g}} \end{pmatrix} \begin{pmatrix} \zeta \\ \xi \end{pmatrix} \tag{5.1}$$

to obtain a system which is diagonal in the highest derivative. The new variables u and v satisfy the equations

$$\begin{aligned} u_t + \frac{1}{6}c_0 h_0^2 u_{xxx} &= -\left(\sqrt[4]{\frac{g}{h_0}}\frac{\partial_x(u-v)}{2} + w_0'\right)\left(u + \sqrt[4]{\frac{h_0}{g}}w_0 + \sqrt[4]{\frac{g}{h_0}}\eta_0 + \sqrt[4]{\frac{g}{h_0}}h_0\right) \\ &\quad -\left(\sqrt[4]{\frac{h_0}{g}}\frac{\partial_x(u+v)}{2} + \eta_0'\right)\left(\sqrt{\frac{g}{h_0}}\frac{u-v}{2} + \sqrt[4]{\frac{g}{h_0}}w_0 + \sqrt[4]{\frac{h_0}{g}}g\right) \\ &\quad -\sqrt[4]{\frac{h_0}{g}}\frac{gh_0^2}{6}\eta_0''' - \sqrt[4]{\frac{g}{h_0}}\frac{h_0^3}{6}w_0''' \\ &\quad \equiv \lambda_u(u, v, \partial_x), \\ v_t - \frac{1}{6}c_0 h_0^2 v_{xxx} &= \left(\sqrt[4]{\frac{g}{h_0}}\frac{\partial_x(u-v)}{2} + w_0'\right)\left(-v + \sqrt[4]{\frac{h_0}{g}}w_0 - \sqrt[4]{\frac{g}{h_0}}\eta_0 - \sqrt[4]{\frac{g}{h_0}}h_0\right) \\ &\quad -\left(\sqrt[4]{\frac{h_0}{g}}\frac{\partial_x(u+v)}{2} + \eta_0'\right)\left(\sqrt{\frac{g}{h_0}}\frac{u-v}{2} + \sqrt[4]{\frac{g}{h_0}}w_0' - \sqrt[4]{\frac{h_0}{g}}g\right) \\ &\quad +\sqrt[4]{\frac{h_0}{g}}\frac{gh_0^2}{6}\eta_0''' - \sqrt[4]{\frac{g}{h_0}}\frac{h_0^3}{6}w_0''' \\ &\quad \equiv \lambda_v(u, v, \partial_x). \end{aligned}$$

The functions u and v also satisfy homogeneous Dirichlet boundary conditions at the endpoints x_1 and x_2 of the computational domain. In addition, we require the Neumann conditions $u_x(x_2,t) = 0$ and $v_x(x_1,t) = 0$. The first and third spatial derivatives are approximated by the matrices $D_{N,1}$ and $D^u_{N,3}$, $D^v_{N,3}$, respectively. The matrix $D_{N,1}$ arises from a standard finite-difference approximation of the first

derivative. The matrix $D^u_{N,3}$ is given by

$$D^u_{N,3} = \frac{1}{2(\delta x)^3}\begin{pmatrix} 10 & -12 & 6 & -1 & & & \\ 2 & 0 & -2 & 1 & & & \\ -1 & 2 & 0 & -2 & 1 & & \\ & \ddots & \ddots & \ddots & \ddots & \ddots & \\ & & -1 & 2 & 0 & -2 & 1 \\ & & & -1 & 2 & 0 & -2 \\ & & & & -1 & 2 & 1 \end{pmatrix}. \tag{5.2}$$

This matrix arises from the use of one-sided Taylor approximations on the left side of the domain, since only one boundary conditions is required there. Since a Neumann condition is given on the right side of the domain, a simpler pattern is seen in the right lower half of the matrix. Similar considerations are applied to construct $D^v_{N,3}$.

The system of ordinary differential equations resulting from the spatial discretization is integrated with a combined Crank-Nicholson Adams-Bashforth method. The linear terms are treated with a Crank-Nicholson method, while the nonlinear terms are treated using an Adams-Bashforth method. This combination of time discretizations is explicit, but treats the highest-order spatial derivatives implicitly. Using the notation U^m_N to denote the N-vector approximating $u(\cdot, m\,\delta t)$ at the m-th time step, and respectively for V^m_N, the equations to be solved at the m-th time step are

$$\begin{aligned} U^{m+1}_N &= (I + c_0 h_0^2 \tfrac{\delta t}{12} D^u_{N,3})^{-1}[(I - c_0 h_0^2 \tfrac{\delta t}{12} D^u_{N,3}) U^m_N \\ &\quad + \tfrac{\delta t}{2}\{3\lambda_u(U^m_N, V^m_N, D_{N,1}) - \lambda_u(U^{m-1}_N, V^{m-1}_N, D_{N,1})\}] \\ V^{m+1}_N &= (I - c_0 h_0^2 \tfrac{\delta t}{12} D^v_{N,3})^{-1}[(I + c_0 h_0^2 \tfrac{\delta t}{12} D^v_{N,3}) V^m_N \\ &\quad + \tfrac{\delta t}{2}\{3\lambda_v(U^m_N, V^m_N, D_{N,1}) - \lambda_v(U^{m-1}_N, V^{m-1}_N, D_{N,1})\}] \end{aligned}$$

As two previous time steps are required to compute the next time step, the very first time step is done using a simple forward Euler method. The Euler method is locally of second order, and a single time step does not lead to instability problems. In Table 4, a convergence study is presented, using an exact solution found in [19]. In non-dimensional variables, where both $g = 1$ and $h_0 = 1$ are set to unity, this solution is given by

$$\begin{aligned} \eta(x,t) &= -\frac{6+\kappa}{12} + \frac{\kappa}{4}\,\mathrm{sech}^2\left(\frac{1}{2}\sqrt{\kappa}(x + x_0 - ct)\right), \\ w(x,t) &= \frac{\mp\sqrt{2}(6+\kappa) + 12c}{12} \pm \frac{\kappa}{2\sqrt{2}}\,\mathrm{sech}^2\left(\frac{1}{2}\sqrt{\kappa}(x + x_0 - ct)\right), \end{aligned} \tag{5.3}$$

for positive κ and c. This exact traveling wave is integrated in time, and it can be seen that second-order convergence is obtained for both the spatial and the temporal

Table 4 Convergence of time and space discretization

δt	L^2-error	L^2-ratio	n	L^2-error	Ratio
2^{-3}	4.53e−03	3.89	3	7.95e−05	3.99
2^{-4}	1.16e−03	3.89	4	1.99e−05	4.00
2^{-5}	2.91e−04	3.96	5	4.95e−06	4.01
2^{-6}	7.22e−05	4.08	6	1.22e−06	4.04
2^{-7}	1.64e−05	4.39	7	2.94e−07	4.17
2^{-8}	4.46e−06	3.67	8	6.45e−08	4.55

The spatial domain is $[-50, 50]$. In the first three columns, the grid size $\delta x = 0.01$ is fixed, and the error is measured at time $t = 1$. In the last three columns, the time step $\delta t = 0.001$ is fixed, and the error is measured at time $t = 1$. The number of grid points N is given by $N = 100 \times 2^n$

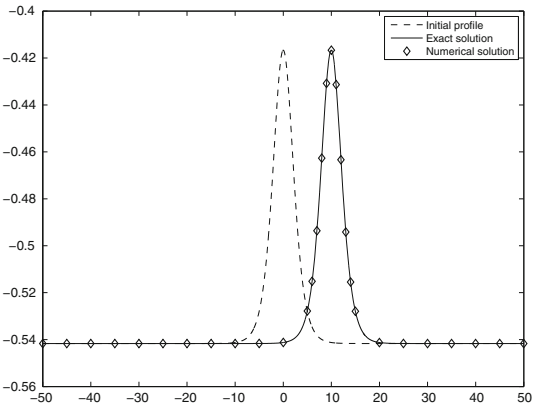

Fig. 5 Plots of η of the exact traveling wave defined in (A-3) with $\kappa = \frac{1}{2}$ and $c = 1$, shown at time $t = 10$. The computed profile was obtained with a resolution $\delta x = 0.01$ and $\delta t = 0.01$

discretization. Figure 5 shows both the initial profile $\eta(x, 0)$ and the computed profile $\eta(x, t)$ at $t = 10$.

References

1. Alazman, A.A., Albert, J.P., Bona, J.L., Chen, M., Wu, J.: Comparison between the BBM equation and a Boussinesq system. Adv. Differ. Equ. **11**, 121–166 (2006)
2. Albert, J.P.: Concentration compactness and the stability of solitary-wave solutions to nonlocal equations. In: Applied Analysis (Baton Rouge, LA, 1996), pp. 1–29. Contemp. Math. vol. 221. American Mathematical Society, Providence (1996)
3. Ali, A., Kalisch, H.: Energy balance for undular bores. C. R. Mecanique **338**, 67–70 (2010)
4. Ali, A., Kalisch, H.: Mechanical balance laws for Boussinesq models of surface water waves. J. Nonlinear Sci. **22**, 371–398 (2012)
5. Benjamin, T.B., Lighthill, M.J.: On cnoidal waves and bores. Proc. R. Soc. Lond. A **224**, 448–460 (1954)
6. Binnie, A.M., Orkney, J.C.: Experiments on the flow of water from a reservoir through an open channel II. The formation of hydraulic jumps. Proc. R. Soc. Lond. A **230**:237–246 (1955).
7. Bjørkavåg, M., Kalisch, H.: Wave breaking in Boussinesq models for undular bores. Phys. Lett. A **375**, 157–1578 (2011)

8. Bona, J.L., Chen, M., Saut, J.-C.: Boussinesq equations and other systems for small-amplitude long waves in nonlinear dispersive media. I. Derivation and linear theory. J. Nonlinear Sci. **12**, 283–318 (2002)
9. Bona, J.L., Colin, T., Lannes, D.: Long wave approximations for water waves. Arch. Ration. Mech. Anal. **178**, 373–410 (2005)
10. Bona, J.L., Dougalis, V.A., Mitsotakis, D.E.: Numerical solution of KdV-KdV systems of Boussinesq equations. I. The numerical scheme and generalized solitary waves. Math. Comput. Simul. **74**, 214–228 (2007)
11. Bona, J.L., Grujić, Z., Kalisch, H.: A KdV-type Boussinesq system: From the energy level to analytic spaces. Discrete Contin. Dyn. Syst. **26**, 1121–1139 (2010)
12. Bona, J.L., Pritchard, W.G., Scott, L.R.: An evaluation of a model equation for water waves. Phil. Trans. Roy. Soc. Lond. A **302**, 457–510 (1981)
13. Bona, J.L., Varlamov, V.V.: Wave generation by a moving boundary. In: Nonlinear partial differential equations and related analysis, pp. 41–71. Contemp. Math., vol. 371, American Mathematical Society, Providence (2005)
14. Borluk, H., Kalisch, H.: Particle dynamics in the KdV approximation. Wave Motion **49**, 691–709 (2012)
15. Byatt-Smith, J.G.B.: The effect of laminar viscosity on the solution of the undular bore. J. Fluid Mech. **48**, 33–40 (1971)
16. Chanson, H.: The Hydraulics of Open Channel Flow. Arnold, London (1999)
17. Chanson, H.: Current knowledge in hydraulic jumps and related phenomena. A survey of experimental results. Eur. J. Mech. B Fluids **28**, 191–210 (2009)
18. Chanson, H.: Undular tidal bores: basic theory and free-surface characteristics. J. Hydraul. Eng. ASCE **136**, 940–944 (2010)
19. Chen, M.: Exact solution of various Boussinesq systems. Appl. Math. Lett. **11**, 45–49 (1998)
20. Constantin, A.: The trajectories of particles in Stokes waves. Invent. Math. **166**, 523–535 (2006)
21. Constantin, A., Strauss, W.: Pressure beneath a Stokes wave. Comm. Pure Appl. Math. **63**, 533–557 (2010)
22. Duruk, N., Erkip, A., Erbay, H.A.: A higher-order Boussinesq equation in locally non-linear theory of one-dimensional non-local elasticity. IMA J. Appl. Math. **74**, 97–106 (2009)
23. Dutykh, D., Dias, F.: Energy of tsunami waves generated by bottom motion. Proc. R. Soc. Lond. A **465**, 725–744 (2009)
24. Ehrnström, M.: On the streamlines and particle paths of gravitational water waves. Nonlinearity **21**, 1141–1154 (2008)
25. Ehrnström, M., Escher, J., Wahlen, E.: Steady water waves with multiple critical layers. SIAM J. Math. Anal. **43**, 1436–1456 (2011)
26. El, G.A., Grimshaw, R.H.J., Smyth, N.F.: Unsteady undular bores in fully nonlinear shallow-water theory. Phys. Fluids **18**, 027104 (2006)
27. Favre, H.: Ondes de Translation. Dunod, Paris (1935)
28. Fokas, A.S., Pelloni, B.: Boundary value problems for Boussinesq type systems. Math. Phys. Anal. Geom. **8**, 59–96 (2005)
29. Henry, D.: Analyticity of the streamlines for periodic travelling free surface capillary-gravity water waves with vorticity. SIAM J. Math. Anal. **42**: 103–3111 (2010)
30. Kalisch, H.: A uniqueness result for periodic traveling waves in water of finite depth. Nonlinear Anal. **58**, 779–785 (2004)
31. Kalisch, H., Bjørkavåg, M.: Energy budget in a dispersive model for undular bores. Proc. Est. Acad. Sci. **59**, 172–181 (2010)
32. Keulegan, G.H., Patterson, G.W.: Mathematical theory of irrotational translation waves. Nat. Bur. Standards J. Res. **24**, 47–101 (1940)
33. Koch, C., Chanson, H.: Unsteady Turbulence Characteristics in an Undular Bore in River Flow 2006, pp. 79–88. Taylor & Francis Group, London (2006)
34. Koch, C., Chanson, H.: Turbulence measurements in positive surges and bores. J. Hydraul. Res. **47**, 29–40 (2009)
35. Lemoine, R.: Sur les ondes positives de translation dans les canaux et sur le ressaut ondule de faible amplitude. Jl. La Houille Blanche. 183–185 (1948)
36. Madsen, P.A., Schäffer, H.A.: Higher-order Boussinesq-type equations for surface gravity waves: derivation and analysis. Phil. Trans. Roy. Soc. Lond. A **356**, 3123–3184 (1998)

37. Peregrine, P.G.: Calculations of the development of an undular bore. J. Fluid Mech. **25**, 321–330 (1966)
38. Rayleigh, Lord: On the Theory of Long Waves and Bores. Proc. R. Soc. Lond. A **A90**, 324–328 (1914)
39. Sturtevant, B.: Implications of experiments on the weak undular bore. Phys. Fluids **6**, 1052–1055 (1965)
40. Svendsen, I.A.: Introduction to Nearshore Hydrodynamics. World Scientific, Singapore (2006)
41. Varlamov, V.: On the initial-boundary value problem for the damped Boussinesq equation. Discrete Contin. Dynam. Syst. **4**, 431–444 (1998)
42. Varlamov, V.: On the spatially two-dimensional Boussinesq equation in a circular domain. Nonlinear Anal. 699–725 (2001)
43. Wei, G., Kirby, J.T., Grilli, S.T., Subramanya, R.: A fully nonlinear Boussinesq model for surface waves. Part 1. Highly nonlinear unsteady waves. J. Fluid Mech. **294**, 71–92 (1995)
44. Whitham, G.B.: Linear and Nonlinear Waves. McGraw-Hill, New York (1975)